# Chilling Out: A Cool Aqueous Environment Promotes the Formation of Gas–Surface Complexes

Stephanie T. Ota and Geraldine L. Richmond*

Department of Chemistry, University of Oregon, Eugene, Oregon 97403, United States

ABSTRACT: SO_2, an important atmospheric pollutant, has been implicated in environmental phenomena such as acid rain, climate change, and cloud formation. In addition, SO_2 is fundamentally interesting because it forms spectroscopically identifiable complexes with water at aqueous surfaces. Vibrational sum frequency spectroscopy (VSFS) is used here to further investigate the mechanism by which SO_2 adsorbs to water at tropospherically relevant temperatures (0–23 °C). The spectral results lead to two important conclusions. SO_2 surface affinity is enhanced at colder temperatures, with nearly all of the topmost water molecules showing evidence of binding to SO_2 at 0 °C as compared to a much lower fraction at room temperature. This surface adsorption results in significant changes in water orientation at the surface, but is reversible at the temperatures examined here. Second, the SO_2 complex formation at aqueous surfaces is independent of aqueous solution acidity. One challenge in previous uptake studies was the ability to distinguish between the effects of surface adsorption as compared to bulk accommodation. The surface and vibrational specificity of these studies make this distinction possible, allowing a selective study of how the aqueous properties temperature and pH influence SO_2 surface affinity.
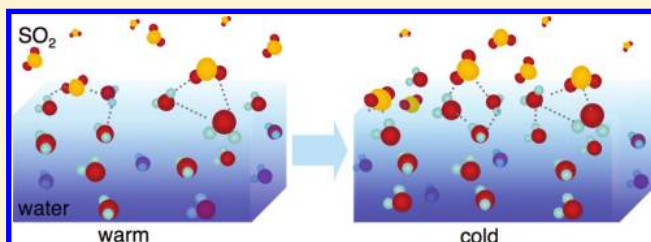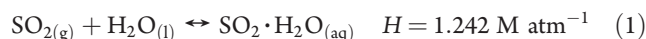
■ INTRODUCTION

The importance of gas uptake to aqueous surfaces in the atmosphere is widely recognized. The congested and often chemically rich environment of aqueous aerosol particles provides a broader range of reactive possibilities than would occur in the gas phase.[1–10] For example, in the gas phase, the primary reaction pathway for atmospheric SO_2 is oxidation by various radicals. Yet in aqueous aerosols the fate of SO_2 depends more on particle composition, which may include reactive species such as aldehydes and ions, in addition to the potential oxidizing agents prevalent in the atmosphere. Other atmospheric gases such as N_2, O_3, Cl_2, HCl, HBr, CH_2O, and NH_3 show similar behavior.[9–11]

We are increasingly learning about the reactivity of atmospheric constituents in gas-phase reactions and in the chemical soup that is comprised within aqueous aerosols, but little is known about the role of the surface separating the two phases. Does it operate as a barrier to reactivity, as a free pathway for entry, or as a temptress that promotes gas uptake? Also, how are interfacial interactions affected by the lower temperature of the atmosphere, which can not only affect surface condensation but also bulk solubility and bulk reactivity? In the absence of reaction, the solubility of most gases is inversely proportional to temperature, but it is unknown whether an increase in bulk solubility at lower temperatures is accompanied by enhanced surface interactions as well. The answers to these types of questions are important for accurately modeling gas uptake and reactivity in the atmosphere.

The aim of this research is to understand the role of temperature and bulk reactivity in the adsorption of atmospherically important SO_2 at a water surface. Uptake of gases such as SO_2 by aerosols depends on many factors including gas-phase diffusion, bulk solubility, mass accommodation probability (the probability of entering the bulk after striking the surface), and bulk reaction rates. Additional complexity arises because all of these factors may be dependent on additional factors such as temperature, pH, and droplet composition.[12–31]

SO_2 reacts with water in a stepwise fashion:[1]

$$SO_{2(g)} + H_2O_{(l)} \leftrightarrow SO_2 \cdot H_2O_{(aq)} \quad H = 1.242 \text{ M atm}^{-1} \quad (1)$$

$$SO_2 \cdot H_2O_{(aq)} \leftrightarrow HSO_3^- + H^+ \quad K_1 = 1.32 \times 10^{-2} \text{ M} \quad (2)$$

$$HSO_3^- \leftrightarrow SO_3^{2-} + H^+ \quad K_2 = 6.42 \times 10^{-8} \text{ M} \quad (3)$$

The dominant reaction product (SO_2 (aq), HSO_3^-, or SO_3^{2-}) depends on the solution pH, but the Henry's law solubility (H) presented in eq 1 does not account for further reaction equilibria. Nor does it attempt to distinguish SO_2 molecules at the surface from those fully solvated in the bulk aqueous phase. Surface species were first invoked to explain discrepancies between mass accommodation measurements and uptake rates calculated from predicted SO_2 solubility and bulk chemistry. Unpredictably high measured SO_2 uptake rates were attributed to surface intermediaries that facilitate gas uptake to water.[18–20,32–40] In bulk water, SO_2 forms a gas hydrate structure with approximately

seven water molecules.[41] This number is expected to be lower at the surface, but the nature of the surface complexes is not well understood.

The role of surface intermediates is also relevant to understanding the results of previous studies that measured the dependence of SO_2 uptake rates on pH and temperature.[12,18,25] These early studies initiated an important discussion regarding whether the effect of higher bulk solubility, via changes in either temperature or pH, is to reduce or enhance surface adsorption and complexation of SO_2. They also highlight the importance of experimental techniques that can investigate surface behavior more directly. The ability to selectively probe surface complexes with water using VSFS provides us the opportunity to begin exploring how SO_2 absorption is coupled to solvation and reaction of the gas in solution.

Recent VSFS experiments confirmed the formation of a short-lived interfacial complex when sulfur dioxide gas interacts with an interfacial solution.[42,43] Using the experimental results in conjunction with MD and ab initio calculations, Baer et al.[44] developed a picture of molecular structure that is consistent with both previous sum frequency measurements of interactions between water and SO_2 at the surface,[42,43] and experimental[45−50] and computational[51−55] studies of behavior in the bulk and at the surface.[44,56] This theoretical study supports the experimentally derived conclusions that, at room temperature, $SO_2(g)$ has a weak affinity for the water surface, forming complexes with water molecules in the topmost interfacial layer. With confirmation of a unique SO_2:H_2O surface complex, the primary question that arises is whether the formation of a surface complex is a necessary step in the uptake of SO_2 to water? Or is it simply a dominant pathway when solubility conditions are less favorable? If these surface complexes are required for uptake, is surface affinity determined by the same factors that determine bulk solubility? Or do physical properties, such as temperature, have different effects on surface affinity than do chemical properties such as pH? Answers to questions such as these are essential to understanding the fate of SO_2 in the atmosphere.

This study provides important answers to many of these questions through experiments that probe SO_2 adsorption on water and aqueous sulfuric acid surfaces at temperatures ranging from 0 to 23 °C. In the first set of experiments, VSFS is used to examine how temperature affects SO_2 complexation at water surfaces for six temperatures between 0 and 23 °C. At each temperature, the OH vibrational stretching region of surface water is examined before, during, and after exposure to SO_2 gas. These VSFS experiments address the question of whether surface affinity increases with bulk solubility as a function of temperature. Isotopic dilution experiments are conducted at 0 °C and, as in previous studies,[57−59] are used as a means of obtaining fitting parameters for the different interfacial environments. Global spectral fitting routines are employed to understand the molecular phenomena reflected in the data, and the results are discussed in the context of recent experimental and theoretical studies, and their implications for the environment. In a second set of studies, the aqueous solution pH is varied to explore the mechanistic questions raised by the previous observation that uptake enhancement varies with solution pH.[18] These experiments are also used to distinguish spectral changes due to adsorption of SO_2 to the water surface from changes due to SO_2 solution reactivity. Changes to the molecular structure and bonding of surface water molecules upon variation of the temperature and pH with the addition of SO_2 are analyzed in reference to the

structure of the neat vapor/water interface. This study culminates in an overview of temperature effects on the SO_2−water system and its relevance to atmospheric systems and aerosol composition.

BACKGROUND

Vibrational sum frequency spectroscopy (VSFS) is well suited to the study of aqueous interfaces, as it is surface specific and forbidden in centrosymmetric media such as bulk water. As a selective vibrational technique, VSFS provides insight into bond strength, orientation, and intermolecular interactions at surfaces, and there are many resources available on the general aspects of the technique.[60−74,74−84]

The sum-frequency intensity is proportional to the square of the second-order susceptibility, $\chi^{(2)}$, which has both resonant and nonresonant components (eq 4). Spectra must be fit to deconvolve the individual resonant modes, a nontrivial task. Employing a fitting routine first proposed by Bain[85] allows us to account for both the homogeneous and the inhomogeneous line widths of the vibrational modes.

$$\chi^{(2)} = \chi_{NR}^{(2)}e^{i\psi} + \sum_{\nu}\int_{-\infty}^{+\infty}\frac{A_\nu e^{i\phi_\nu}e^{-[\omega_L - \omega_\nu/\Gamma_\nu]^2}}{\omega_L - \omega_{IR} + i\Gamma_L}\,d\omega_L \quad (4)$$

The first term in eq 4 is the nonresonant second-order susceptibilty. The second term is a sum over all resonant vibrational modes and is represented as $\chi_{R(\nu)}^{(2)}$. The resonant susceptibility, $\chi_{R(\nu)}^{(2)}$, is proportional to N, the number of molecules contributing to the sum frequency response, and $\langle\beta_\nu\rangle$, the orientationally averaged molecular susceptibility:

$$\chi_{R(\nu)}^{(2)} = \frac{N}{\varepsilon_0}\langle\beta_\nu\rangle \quad (5)$$

The second term in eq 4, the resonant susceptibility (eq 5), is fit as a convolution of the homogeneous line widths of the individual molecular transitions (HWHM, Γ_L) with inhomogeneous broadening (fwhm, $(2\ln 2)^{1/2}\Gamma_\nu$). The transition strength A_ν is proportional to the product of the number of contributing molecules and their orientationally averaged IR and Raman transition probabilities. The frequencies of the IR, the Lorentzian, and the resonant modes are ω_{IR}, ω_L, and ω_ν, respectively. The phase of each resonant mode is ϕ_ν. The intensities of sum frequency spectra are complicated, and changes can arise from changes in the number of contributing molecules, changes in orientation, and/or a change in bond energies.

EXPERIMENTAL SECTION

Laser System. The laser system used in these experiments has been described extensively in previous publications.[40,86,87] Recent modifications to improve the stability and performance of the system will be detailed here. Production of the 800 nm beam used for both the IR generation and the experiment begins with a Ti:Sapphire (Coherent Mira) passively mode-locked laser pumped with 5.5 W of a 532 nm laser beam from a Coherent Verdi laser. The resultant ~135 fs, 800 nm light is used to seed a Ti:Sapphire amplifier (Spectra Physics Spitfire Pro XP) pumped with 15 W of 527 nm light (Spectra Physics Empower Laser), which produces a 2.6 ps beam at 800 nm (1kHz repetition rate). The resultant 2.2 W is split by a 75/25 beam splitter; 25% is available for direct use in the VSF experiments, and the remaining 75% is used to generate the tunable IR. The IR generation system has not been modified. Sum frequency light is generated by overlapping 800 nm

7498

dx.doi.org/10.1021/ja201027k |*J. Am. Chem. Soc.* 2011, 133, 7497–7508

(∼2.6 ps, 1 kHz repetition rate) and tunable (2700−4000 cm^{-1}) infrared light in a copropagating geometry at 56° and 67° from the surface normal, respectively. After filtering any reflected 800 nm light, the resultant sum frequency light is collected with a thermoelectrically cooled CCD camera (Princeton Instruments). All of the spectra presented and discussed here were taken using either the ssp- or sps-polarization schemes, which denote the sum-frequency, visible, and infrared polarizations, respectively.

To minimize contamination, samples are poured into scrupulously clean glass dishes contained in a nitrogen purged Kel-f cell fitted with CaF$_2$ windows. The Kel-f cell has three gas ports, two of which are used for gases, and the remaining port is vented via Teflon tubing to a fume hood. There is an additional port to accommodate a clean Teflon-coated Type T thermocouple probe, which is used to monitor sample temperature. Data collection is facilitated using a Lab View program that records CCD intensity and monitors temperature for each data point. Temperature is continuously monitored to ensure that the sample variation is within 1 °C for each data set, and the temperature is recorded before and after each scan.

Sample Preparation and Analysis. Gases were purchased from AirGas, argon (cylinder, 99.9%), nitrogen (cylinder), and Air Liquide, SO$_2$ (lecture bottle, 99.99%). H$_2$SO$_4$ (5 M volumetric solution), H$_2$SO$_3$ (reagent grade), and HCl were purchased from Aldrich and used as received. High purity water was obtained from a Barnstead E-pure system (18 MΩ cm). Sum frequency intensities were measured using a thermoelectrically cooled CCD camera with a 2 s exposure time. Intensities were recorded in 3 cm^{-1} steps over a range from 2800 to 3900 cm^{-1}. Gas flow experiments were conducted at atmospheric pressure with a constant SO$_2$ gas flow rate of 10 standard cubic centimeters per minute (sccm).

Sum frequency data are normalized to account for spatial variation between the visible and IR while scanning the IR frequency, temporal lengthening of IR pulses by water vapor, absorption of IR energy by SO$_2$ and/or water vapor, and the frequency dependence of the optics used for filtering the SF light. In these experiments, SF spectra were divided by the nonresonant response from an uncoated gold surface. Spectra presented are averages of 3−12 spectra taken over multiple days to ensure reproducibility and to reduce the signal-to-noise ratio.

The parameters used to fit the neat vapor/water interface in ssp-polarization were determined in previous isotopic dilution studies.[57,88,58] Each resonant peak contains five variables (eq 4); thus there may be nonunique fitting solutions. To reduce the number of variables associated with the fits, the phases are fixed at either π (for peaks between 3200−3600 cm^{-1}) or 0 (for peaks below 3200 or above 3600 cm^{-1}); Lorentzian widths are fixed at either 12 cm^{-1} (for the free OH) or 5 cm^{-1} for the remaining OH stretches; and global fitting routines are employed to constrain parameters where possible. The global fitting routine iteratively fits the data while constraining peak positions and Gaussian widths such that the only variables for different samples are the peak amplitudes, lending higher confidence to the results. Global fits to isotopic dilution data taken at 0 °C were performed for each of the solutions prior to, during, and after exposure to SO$_2$ gas. To account for changes due to perturbation by gas flow or ions, spectra were first fit using the same parameters used for the neat water system, allowing only amplitudes to vary. Additional peaks were only added if they were both phenomenologically reasonable and necessary to achieve good agreement between the fits and the spectral response. Peak parameters obtained through the isotopic dilution study are consistent with those used by Tarbuck et al.[43,59] and provide the initial values for subsequent fits to the data taken over a range of temperatures from 0 to 23 °C. The temperature dependent data are fit twice: first using a global fitting routine across the temperature series and then as individual data sets to account for variations in peak positions and widths that might result from changes in temperature. Details about the results and interpretation of these fits are the focus of the ensuing discussion.
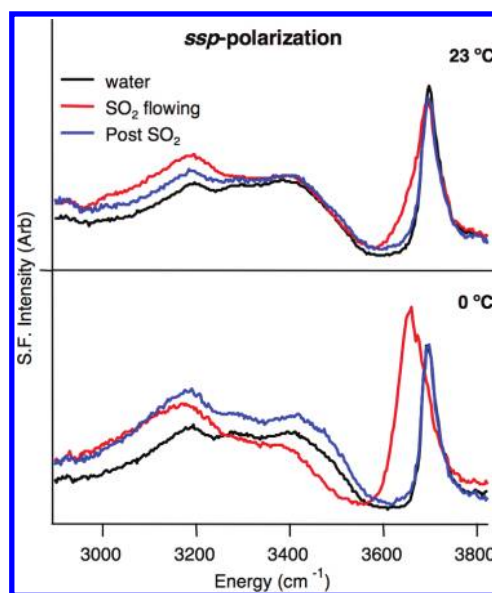

Figure 1. The ssp-polarization spectra of the water OH stretching region before (black), during (red), and after (blue) exposure to SO$_2$ gas at 23 °C (top) and 0 °C (bottom).

RESULTS AND DISCUSSION

Uptake of SO$_2$: The Importance of Temperature. When SO$_2$ gas comes into contact with liquid water, it forms a surface complex that has recently been detected spectroscopically via an examination of the interfacial VSF spectrum of water.[42,43] The data in Figure 1 (top) provide the evidence for this surface complex formation as was originally measured at 23 °C by Tarbuck et al.[42] These spectra correspond to the interfacial OH stretching region of water before (black), during (red), and after (blue) exposure to SO$_2$ gas. One of the most distinct changes to these spectra is the broadening of the sharp peak near 3700 cm^{-1} that occurs only in the presence of flowing SO$_2$ (red). This broadening has been attributed to enhanced coordination between water molecules at the topmost surface layer complexing to SO$_2$.[42,43] In these earlier studies, the surface complex between SO$_2$ and the "free-OH" mode of water was found to be short-lived at room temperature, as it does not persist if the SO$_2$(g) is purged from the system (Figure 1 (blue)). Surface exposure is accompanied by an irreversible intensity increase in the coordinated water region below ∼3400 cm^{-1}, an effect that has been attributed to solvated SO$_2$ and its reaction with water (eqs 1−3). These previous studies demonstrate that SO$_2$ forms reversible surface complexes with water, and these complexes can be probed directly using VSFS. These surface complexes are believed to involve a single SO$_2$ molecule interacting with 1−3 water molecules in the topmost layer of the interfacial region.[42−44]

Figure 1 (bottom) shows recently acquired spectra for SO$_2$ adsorption at a water surface maintained at 0 °C. Visual inspection of data taken at 0 °C shows more dramatic broadening of the 3700 cm^{-1} peak upon exposure to SO$_2$, indicative of enhanced surface complexation at the lower temperature. However, as with the higher temperature, this adsorption is reversible. Spectra taken in the sps-polarization scheme (Figure 2) show similar trends, with increased intensity in the 3700 cm^{-1} region upon exposure to SO$_2$ when the temperature is decreased.
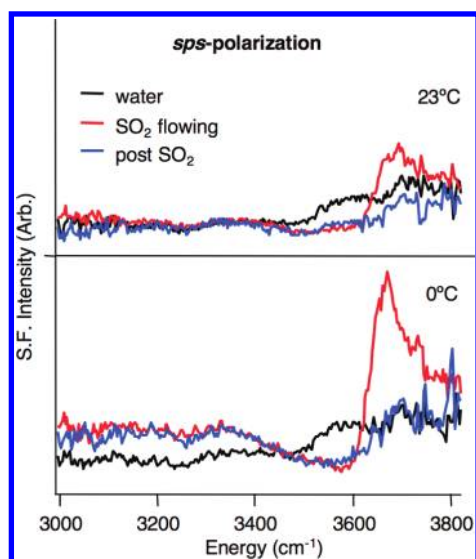
Figure 2. The sps-polarization spectra of the water OH stretching region before (black), during (red), and after (blue) SO_2 exposure at 23 °C (top) and 0 °C (bottom).

Understanding the contributions to the spectral changes observed in Figures 1 and 2 requires more detailed studies as described below. Our approach is to employ isotopic dilution studies for the neat vapor/water interface at 0 °C (Figure 3), followed by identical studies conducted in the presence of SO_2 (Figure 5). Any conclusions drawn from the spectral changes observed must take into account that intensity increases can reflect changes in orientation, population, and/or transition strength of the surface species being measured.

Temperature and the Neat Vapor/Water Interface. It is difficult to represent the molecular environment found at the vapor/water interface in simple terms, and researchers continue to modify and elaborate on the details of its molecular structure and hydrogen bonding.[57,88−115] Assignment of particular water bonding geometries, coordination, and strengths to a specific spectral feature is fraught with difficulty because of the continuum nature of surface water bonding, as well as collective behavior. Nevertheless, past experimental and computational results by a number of groups point to a dominance of particular species in localized interfacial regions. In general, the vapor/water interface can be described as a relatively narrow interfacial region, ∼6−9 Å, where the average coordination of water molecules increases from ∼2 bonds per molecule at the topmost surface layer to ∼3.6 bonds per molecule in the bulk.[95,57,96,115] Molecules with less coordination and fewer hydrogen bonds reside in the topmost water region, which is the easiest to interpret, and vibrate at higher frequencies (3500−3700 cm^{-1}). The highest level of coordination in the interfacial region is for the deeper tetrahedrally coordinated molecules corresponding to lower frequency vibrations (3100−3500 cm^{-1}).

We rely on a combination of spectral fitting and MD calculations to develop an overall picture that allows us to categorize interfacial response in terms of water orientation, coordination, and hydrogen bonding. The neat vapor/water spectral assignments used in this study are based on previous isotopic dilution experiments[57,59,88] and MD simulation results from our laboratory,[102,104] and additional considerations from other studies.[73,92−99,115−117] A representative fit to the neat vapor/water interface at room
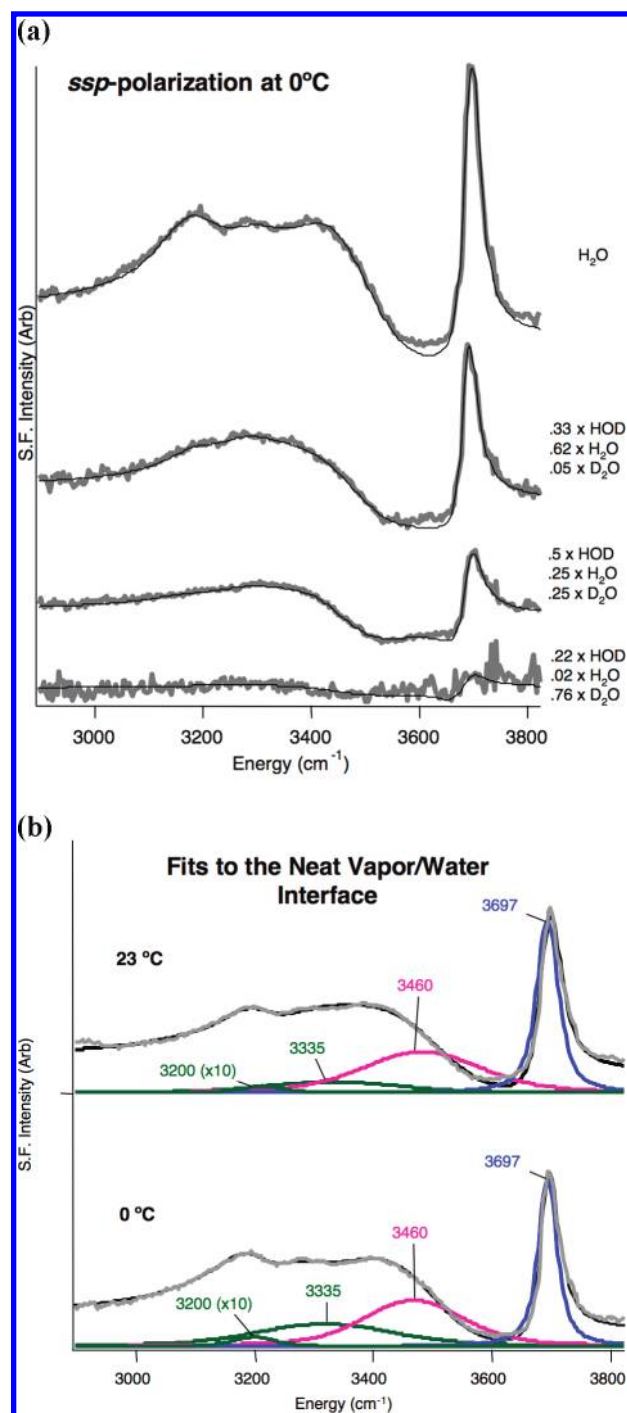

Figure 3. (a) Isotopic dilution series of water at 0 °C. Spectra are offset for clarity. Fits to the data (gray) are in black. (b) Overall fits (black) to the neat vapor/water interface (gray) and resonant components (colored), at 23 °C (top) and 0 °C (bottom).

temperature is shown in Figure 3b (top), along with its component resonant features (colored). For simplicity, spectral contributions are described as arising from four dominant water environments, but each mode is actually comprised by contributions from several types of OH stretching environments.

The description of the vapor/water interface that is referred to throughout this study is as follows: (I) The free OH peak, at ∼3700 cm^{-1}, is attributed to unbound OH oscillators with an

average orientation away from the bulk. This mode protrudes out of the surface and is highly sensitive to weakly bound species at the surface. (II) The mode opposite the free OH mode (the companion OH) points into the bulk and gives rise to broad spectral intensity at ~3460 cm^{-1}, a frequency consistent with measurements of the OH of uncoupled HOD in liquid water.[116] MD calculations support this conclusion and go further to indicate that such highly oriented water molecules interact weakly with neighboring molecules via hydrogen bonds through both the hydrogen and the oxygen.[94,102,104] Small contributions to this peak can also come from loosely coupled water molecules in the more coordinated region of the interface. (III) Loosely bound water molecules that are mostly parallel to the interface are observed at ~3580 cm^{-1} and primarily contribute to data taken in the sps-polarization scheme.[94,104] (IV) Slightly deeper in the interfacial region, one finds more coordinated water molecules, sometimes referred to as tetrahedrally bound water, which give rise to two modes at ~3335 and ~3200 cm^{-1}. The assignment of the intensity at 3200 cm^{-1} has recently been attributed to a Fermi resonance between the overtone of the water bending mode and the fundamental of the water symmetric stretch mode, reigniting the debate over peak assignments in the water region.[92,93,118,119] While discussion over the specific molecular origins of this intensity continues, the consensus from isotopic dilution studies of the OD[92,93] and OH[57,59,88] stretching regions and recent MD simulations[104] is that the intensity of this mode increases with more extensive hydrogen bonding and increased intermolecular coupling.

The recent development[120] and implementation of phase-sensitive sum frequency measurements by a number of groups has raised questions about how sum frequency spectra, particularly of water, are fit.[73,97-99,107,108,117] The main discrepancy between the recent phase measurements and the parameters we use to fit the water spectra is in the phase of the lower frequency region. Measurements by the Shen group detect a phase change below 3200 cm^{-1} that was not previously included in fits to the vapor/water interface.[73,97-99,117] We find that we can incorporate this phase change by adding an additional mode, but its amplitude is negligible for the neat vapor/water interface. Upon the addition of ions or gas to the interface, the intensity of this peak increases and is taken into account when appropriate. This interpretation is consistent with a recent MD study that indicates the apparent phase change results from the anisotropic contribution to the polarizability, which increases in stronger hydrogen-bonding environments.[107,108] Similarly, previous VSF studies of strong acids[121] and the vapor/ice interface[122-124] attributed a peak at ~3150 cm^{-1} to more water coordination and stronger hydrogen bonding.

Isotopic Dilution. Prior to examining the influence of temperature on the uptake of sulfur dioxide to water, it is important to establish a baseline and fitting parameters for the VSFS response from the vapor/water interface at 0 °C in the absence of SO_2. As mentioned previously, isotopic dilution experiments have successfully been used in the past to isolate resonant components in the water OH stretching region at room temperature.[57,59,88] Adding D_2O increases the HOD concentration, which simplifies the sum frequency response by reducing the effects of intra- and intermolecular coupling. These solutions also provide us with spectral constraints, because the OH stretching region for each solution must be fit using the same parameters. The isotopic dilution experiments for water at 0 °C are presented in Figure 3a. The resultant fits to the data confirm that the
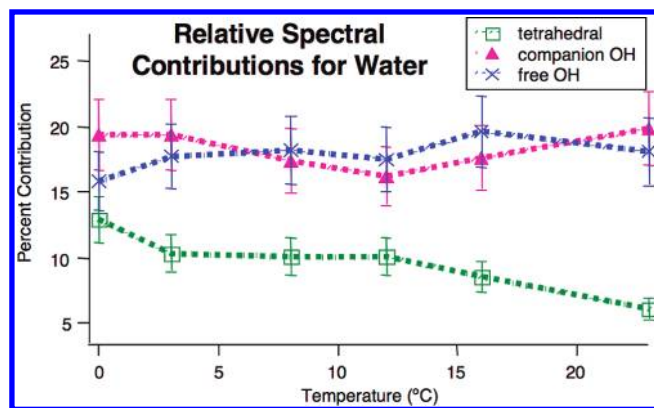

Figure 4. Relative contributions of fitted OH stretching regions as a function of temperature.

previously determined fitting parameters for the neat vapor/water interface still apply at 0 °C. The overall fits and the component resonant modes for water are shown in Figure 3b at 23 °C (top) and 0 °C (bottom).

In conjunction with the isotopic dilution series at 0 °C, spectra of the neat vapor/H_2O interface were also obtained at 3, 8, 12, 16, and 23 °C. Figure 4 shows how the relative contributions from different OH stretching regions change with temperature. The relative contributions were calculated on the basis of the peak areas for the resonant components as a percentage of the area of the overall fit. The tetrahedral region reflects the combined area of the peaks at 3200 and 3335 cm^{-1}. Percent errors were estimated for each temperature based on standard deviations in the fitted amplitudes for multiple data sets. These percentages (ranging from 5% to 30%) were applied to the peak areas calculated for the averaged data sets. Characterizing the interfacial response in this manner allows us to investigate trends and changes with respect to water coordination and orientation when the temperature changes and/or gases or solutes are added. This facilitates our ability to determine which spectral regions are affected by a surface perturbation. For example, through changes in the tetrahedral region, we can infer information about how the perturbation affects the most strongly coordinated molecular resonances somewhat deeper in the interface.[104] By contrast, changes in the free OH region are a clear indication that the topmost water layer is being perturbed.

From the results in Figures 3 and 4, the behavior of the neat vapor/water interface parallels that of bulk water, with increased coordination as the temperature decreases. The most notable difference as the temperature decreases is an increase in the amplitudes of the peaks at 3200 and 3335 cm^{-1}. Their spectral contribution grows when the temperature approaches that of ice, while the contribution from the free and companion OH modes is relatively constant over the temperature range studied. The small changes to the water spectra shown in Figure 3b are consistent with changes reported by earlier studies at 0 °C,[122-124] which showed a similar increase in the relative contribution from more highly coordinated OH stretching. As there are no changes in the overall electric field or composition of these solutions, the increased intensity of the tetrahedral mode is most likely due to an increase in the net water orientation as the temperature approaches that of ice. These interfacial changes seem small in view of the large spectral changes we observe when $SO_2(g)$ is introduced to the system (Figure 1), but they provide us with the
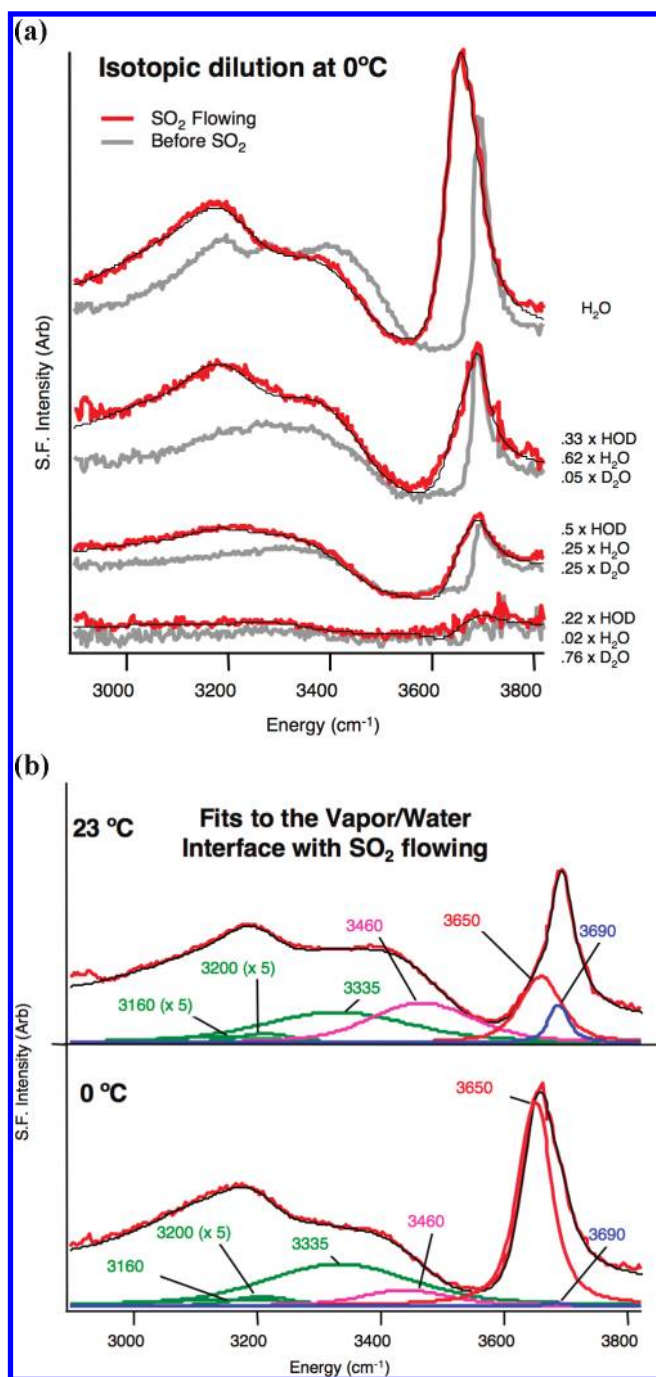
Figure 5. (a) Isotopic dilution series at 0 °C with SO$_2$ flowing (red) with corresponding water solutions (gray). (b) Fits (black) to the OH stretching region with SO$_2$ gas flowing (dark red) and resonant components (color) at 23 °C (top) and 0 °C (bottom).

Figure 6. (a) The ssp-spectra of the water OH stretching region with SO$_2$ flowing (color) and corresponding fits (thin black) as a function of temperature. The neat vapor/water interface at corresponding temperatures is in gray. (b) Relative contributions of fitted OH stretching regions as a function of temperature.

basic parameters necessary to begin analyzing the SO$_2$/water system.

SO$_2$ at the Vapor/Water Interface: The Effects of Temperature. The adsorption behavior of SO$_2$ at the cold water surface (Figures 1 and 2) was investigated using isotopic dilution experiments and global fitting routines. An analysis similar to that used for water in Figure 3 was applied to analyze spectra taken while flowing SO$_2$ gas over the water surface. The isotopic dilution series used to determine the fitting parameters for
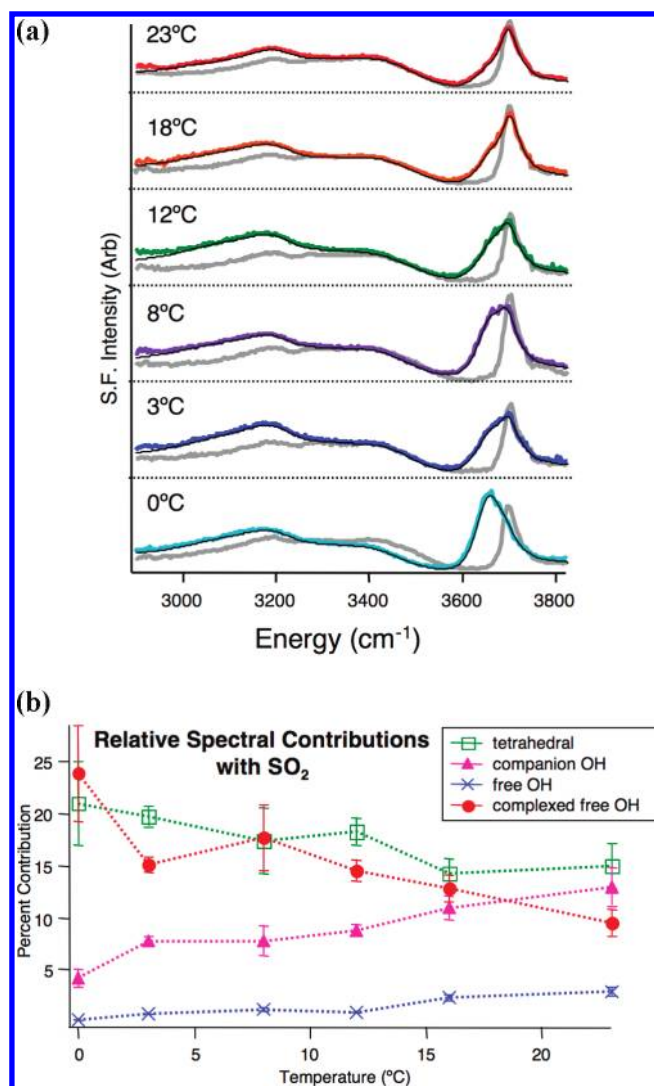
spectra obtained with SO$_2$ flowing at 0 °C is shown in Figure 5 (red), with corresponding water data (gray) for reference. From these data, we observe two main spectral changes: a broadening of the mode at ~3700 cm^{-1} and increased intensity below ~3400 cm^{-1}. Fits to spectra taken while SO$_2$ gas is flowing cannot be achieved using only the standard four water bands. Two additional contributions are included to obtain an accurate global fit to the data in Figures 1, 5, and 6; a sharp peak attributed to surface complexes with molecular SO$_2$ at ~3650 cm^{-1}, which will be referred to as the complexed free OH, and a small broad peak at ~3150 cm^{-1} that is likely due to enhanced OH coordination. These two peaks, in combination with the four water peaks, form the basis for the global fit used to interpret the spectral changes observed as a function of temperature. Lowering the temperature accentuates the spectral changes observed when the water surface is exposed to SO$_2$ at room temperature, proving that more surface adsorption occurs at colder temperatures. This surface enhancement can be seen in Figure 6, which shows how

the OH stretching region of water (gray) evolves when SO_2 is flowing (color) at intermediate temperatures between 0 and 23 °C.

In the initial analysis, three different approaches were used to fit the high frequency region above ∼3600 cm^{-1}, all of which lead to the same conclusion regarding the free OH region. These approaches are as follows: including peaks at ∼3650 and ∼3700 cm^{-1} and varying their amplitudes while holding their frequencies and widths constant with temperature; treating the peak as a single resonant peak that varies in both frequency and width as the temperature decreases; or fixing the frequency of the ∼3700 cm^{-1} peak and varying the frequency and width of the peak at ∼3650 cm^{-1}. For all three approaches, the net result is that the integrated intensity of this high frequency region increases as the temperature decreases.

For the analysis discussed below, we apply the first approach, holding the frequency and width constant, as it provides the best fit to the data in Figures 5 and 6 while limiting the number of variable parameters and giving a measurable indicator of complex formation. This approach is consistent with the picture that the surface spectra in this region are comprised of an unbound free OH peak and a lower energy peak corresponding to a $SO_2:H_2O$ surface complex. The lower energy peaks were fit using the parameters described above. The resultant fits obtained using a global fitting analysis are shown in Figure 5b with the corresponding resonant contributions (color) for data taken at 23 °C (top) and 0 °C (bottom). The relative contributions from the resonant peaks are displayed in Figure 6b as a function of temperature. The companion OH, free OH, and complexed free OH peaks are at ∼3460, ∼3690, and ∼3650 cm^{-1}, respectively. The tetrahedral OH region on this plot refers to the combined contributions from the peaks at 3160, 3200, and 3335 cm^{-1}.

As shown in Figure 5b, when the temperature reaches 0 °C, the contribution from the peak at ∼3650 cm^{-1}, which is attributed to water complexed to SO_2, increases significantly. Meanwhile, the contribution from the peak at 3700 cm^{-1} becomes almost negligible. The observed bonding of SO_2 to essentially all of the free OH bonds leads us to conclude that under low temperature conditions, the topmost surface region is fully involved in SO_2 complexation. The shift in intensity from the uncomplexed to the complexed free OH peak is attributed to an increase in surface SO_2 adsorption in conjunction with a change in overall water orientation as more water molecules bind to SO_2. Support for this interpretation comes from data obtained using the sps-polarization scheme, which probes vibrations with components of the dipole in the plane of the interface (Figure 2). Rigorous spectral fitting in the sps-polarization scheme is difficult due to the high nonresonant background relative to the resonant signal for these experiments, but approximate fits were obtained using parameters similar to those used for data obtained in the ssp-polarization scheme. The main difference from the ssp-data is that loosely bound water molecules lying nearly parallel to the interface give rise to a peak at ∼3580 cm^{-1} for the neat interface (black) that decreases significantly upon addition of SO_2 (red), becoming negligible when the temperature reaches 0 °C. The intensity decrease at ∼3580 cm^{-1} accompanies a corresponding intensity increase at ∼3650 cm^{-1}, similar to that seen in the ssp-data. These data indicate that the surface adsorption of SO_2 acts to reorient loosely coordinated water molecules in the topmost interfacial layer such that their OH oscillators are tilted more out of the plane of the interface, a change that is greatly enhanced at lower temperature.

The recent MD work by Baer et al. suggests that SO_2 adsorption induces both reorientation and increased cooperation between surface water molecules.[44] Their simulations indicated that SO_2 forms complexes with multiple water molecules, with multiple coordination geometries consistent with a red-shifted free OH peak. The spectral implications of forming multiwater surface complexes are expected to extend below the free OH region. The peak at ∼3460 cm^{-1} reflects contributions from the companion OH bonds of the water molecules containing free OH, as well as from loosely bound water molecules in the topmost surface layers.[104] In both the ssp- and the sps-polarization schemes, the integrated area of this peak decreases upon addition of SO_2 gas, and its overall spectral contribution decreases further with increased SO_2 bonding as the temperature decreases. The complexation of SO_2 to loosely bound water molecules in the interfacial region and tighter water coordination results in a red-shift of intensity away from this peak.

Thus far, we have determined that cooler temperatures lead to increased surface accumulation of SO_2, but do these changes extend deeper into the interface, as well? The solubility of SO_2 increases at lower temperatures, driving increased production of both HSO_3^- and H^+ via the reactions shown in eqs 1–3. The spectral increases exhibited in the lower frequency tetrahedral region are consistent with increased ion concentrations, which induce greater water coordination. Both $HSO_3^{-[43]}$ and $H^{+[59,125-127]}$ are expected to accumulate in the interfacial region and elicit similar spectroscopic responses, an increase in the intensity below ∼3400 cm^{-1}. HSO_3^- is a relatively large polarizable anion capable of hydrogen bonding to water via strong ion—dipole interactions, and protons are known to elicit strong electrostatic interactions. Figure 6b shows an increase in the contribution from tetrahedrally coordinated OH oscillators when the temperature is decreased. This is consistent with the increased coordination and electric field expected at higher HSO_3^- and H^+ concentrations. On the basis of these observations, the changes to the deeper, more coordinated water layers are consistent with the expected increase in SO_2 solubility at lower temperature. To confirm that these lower energy intensity changes are due to solvated species, and not the surface complexes themselves, we examine the uptake of SO_2 to acidic solutions.

Uptake of SO_2 at Low pH. As discussed above, there is considerable ambiguity regarding the nature of SO_2 surface complexation under the acidic conditions relevant to aerosol chemistry. Some studies report unpredictably high uptake rates as compared to expected bulk reactivity, indicating that surface complexes may be important;[15,18] another study indicates that surface reactions are insignificant at high H_2SO_4 concentrations.[25] The surface accommodation of SO_2 to 2.5 M sulfuric acid solutions was examined to provide insight into these issues. To ensure that the results were not dependent on the type of acid used, the experiments were repeated using HCl to adjust the solution pH. Similar results were also obtained using aqueous solutions that were made highly acidic with SO_2. Under low pH conditions, the uptake of SO_2 into the bulk solution should be significantly lowered, because the formation of HSO_3^- is unfavorable.[23–25,34] Hence, these pH studies provide us with a mechanism for removing the ambiguity of previous results, while also elucidating the surface behavior upon inhibiting the reactive channel following uptake.

Figure 7 shows VSF spectra of 2.5 M H_2SO_4 solutions obtained before (light blue), during (red), and after (dark blue) exposure to SO_2 at 23 °C (top) and 0 °C (bottom). For
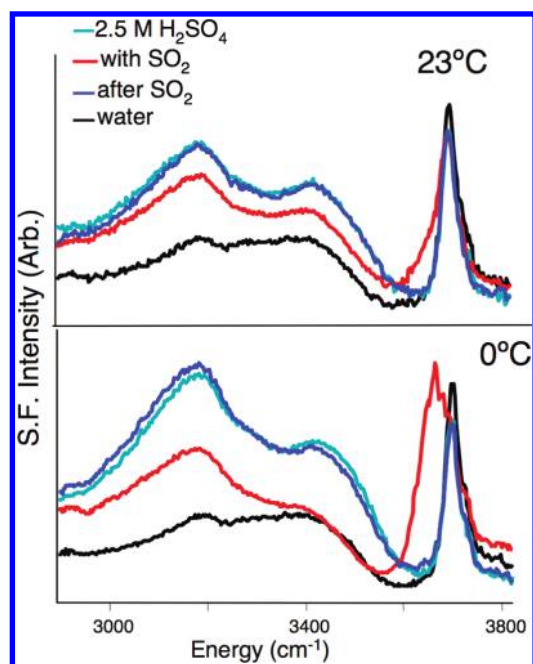
Figure 7. 2.5 M H_2SO_4 at 23 °C (top) and 0 °C (bottom). The ssp-spectra were obtained before (light blue), during (red), and after (dark blue) exposure to SO_2. Acid-free water (black) is shown for comparison.

reference, the vapor/water interface without added H_2SO_4 is shown in black for each of these systems. Visual inspection of the data in Figure 7 shows that at both temperatures, surface complexation occurs even in the presence of high bulk concentrations of H_2SO_4, as manifested in the broadening of the free OH upon exposure to SO_2 (red), a broadening that is accentuated at lower temperature (bottom). Once the SO_2 is removed, the VSF spectra (dark blue), at both temperatures, are essentially identical to those taken before adding SO_2 (light blue). This confirms that the surface chemistry is different from that of acid-free water (Figure 1), where the effects of interfacial HSO_3^- ions are observed in the 3200 cm^{-1} spectral region after removal of SO_2 from the system.

To obtain a more detailed picture of these effects, spectral fitting analyses were performed for the H_2SO_4 data in Figure 7. Figure 8a and b contains the fitting results for the H_2SO_4 solutions prior to flowing SO_2 (light blue) and upon exposure to SO_2 (red), respectively, at 0 °C (bottom) and 23 °C (top). Focusing first on the H_2SO_4 solutions in the absence of SO_2, Figure 8a, the 2.5 M H_2SO_4 differs from the acid-free water spectrum by a larger VSFS response below ~3400 cm^{-1} and a slight decrease in the free OH contribution at both temperatures. These results are consistent with previous VSF studies of H_2SO_4 solutions.[128−134] When compared to neutral water, the main differences found from the fitting analysis are that for the acidic solution the peak at 3200 cm^{-1} is much larger, and there is an additional peak at 3150 cm^{-1} that is attributed to highly coordinated water molecules with increased hydrogen-bonding interactions. Overall, these spectral changes reflect that the H_2SO_4 containing solution has a more structured water surface with orientation that extends deeper into the interfacial region. This is consistent with a molecular picture where solvated ions in the bulk induce an electric field that extends toward the water surface. At lower temperature, the amplitude increase at 3200 cm^{-1} is even more pronounced, consistent with an even greater increase in water coordination.
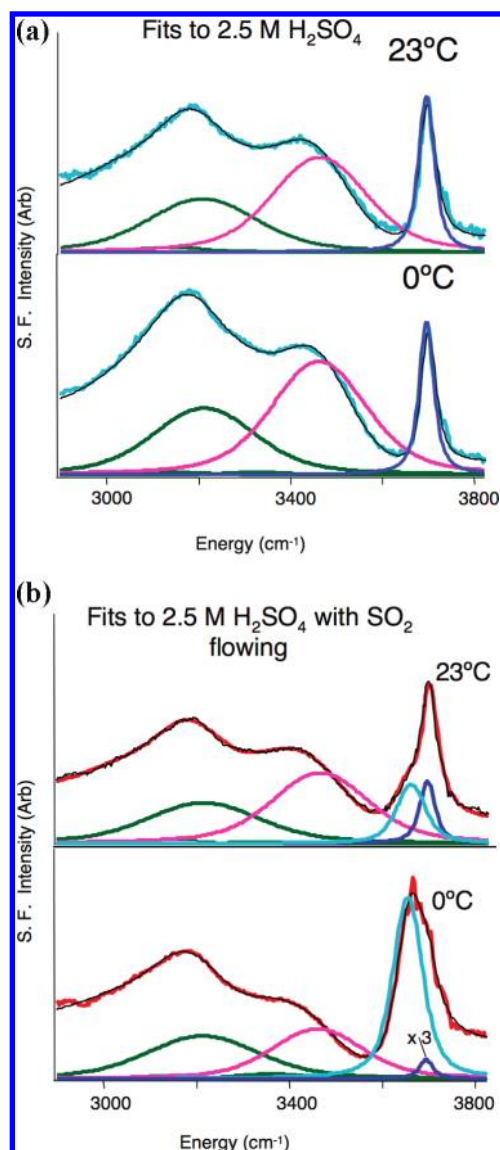

Figure 8. (a) The overall fit (thin black) and resonant components (colored) for H_2SO_4 (light blue) at 23 °C (top) and 0 °C (bottom). (b) The overall fit (thin black) and resonant components (colored) for H_2SO_4 with SO_2 flowing (red) at 23 °C (top) and 0 °C (bottom).

A similar analysis of the H_2SO_4 solution surface in the presence of SO_2 shows both similarities and differences when compared to the analysis of SO_2 at the acid-free water surface. A comparison of the data in Figure 8a and b shows that the surface complex on the acid solution is manifested in spectral changes in the free OH peak similar to those observed for the neutral solution in Figure 5, increased broadening and red-shifting of this peak when the temperature is lowered and complexation is increased. SO_2 complexation on the H_2SO_4 surface is also demonstrated by the decrease in the nearby companion OH mode, which is evident in the decreased contribution from the peak near 3500 cm^{-1} in Figure 8a and b. As for the neutral solution, this decrease upon exposure to SO_2 is attributed to an increase in the coordination and net orientation of loosely coordinated water molecules in the topmost interfacial layer. The highly coordinated region below 3400 cm^{-1} is where the spectra of the acidic and neutral solutions differ upon exposure to SO_2. The acidic
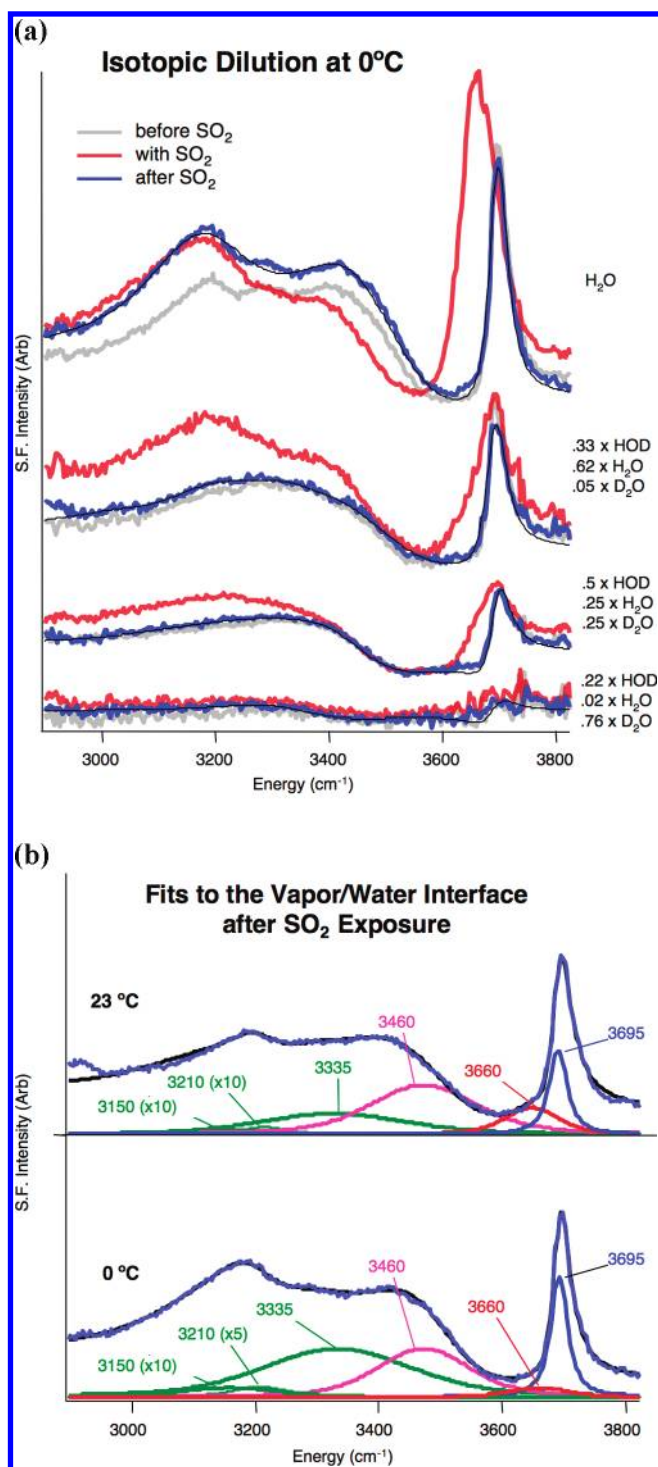
Figure 9. (a) Isotopic dilution series taken after purging SO_2 from the system (blue) with corresponding spectra taken before (gray) and during (red) SO_2 exposure. (b) Resonant modes and fits to spectra of the vapor/water interface after exposure to SO_2 at room temperature (top) and 0 °C (bottom).

Figure 10. Relative contributions of the fitted OH stretch region, after exposure to SO_2, as a function of temperature.

production of HSO_3^- ions. The contrasting behavior observed here provides further evidence that, under acidic conditions, the adsorption of SO_2 is localized to the topmost water layer and the level of solvated SO_2 and HSO_3^- in the interfacial region is negligible. As a whole, these measurements provide a means of distinguishing between surface water binding to SO_2 and changes due to solvated ions in the interfacial region.

On the basis of these results, the conditions that dictate interactions between SO_2 and H_2O at the surface are uncoupled from those that determine behavior in the bulk. As the data in Figure 7 show, SO_2:H_2O surface complexes continue to form under acidic conditions, clarifying the ambiguous results of previous studies that could not distinguish between surface and bulk interactions.[15,18,25] Similar to the behavior at the neat water surface, SO_2 surface complexation is enhanced at lower temperatures and occurs regardless of bulk absorption behavior. Further, the surface complexes are localized to the topmost surface layer, with little influence on the deeper interfacial region. The lower energy spectral region reflecting deeper more coordinated water molecules is thus an ideal indicator of solvated species such as HSO_3^-.

The Vapor/Water Interface after Exposure to $SO_2(g)$. As noted earlier, after SO_2 is absorbed by water it reacts to form HSO_3^- in solution (eq 2). A decrease in temperature corresponds to an increase in SO_2 solubility, shifting this reaction to produce higher levels of HSO_3^-. The SO_3^{2-} concentration is expected to be negligible under these pH conditions. Figure 1 (blue) shows that when SO_2 is removed the free OH mode returns to its original narrow state, but there is a large increase in the intensity below 3600 cm^{-1}, which is enhanced as the temperature decreases. The sps data support the reversibility of these surface interactions; the peak at ~3580 cm^{-1} must be included to fit the high energy spectral region in Figure 2 (blue). As confirmed by isotopic dilution (Figure 9a), the post-SO_2 ssp-spectra can be fit using six peaks: the same four parameters used for water with a small peak at 3150, which is attributed to more coordination between water molecules, and a small peak at 3660 cm^{-1} that is attributed to water solvating interfacial protons and HSO_3^- (Figure 9b). The solvation mode is much broader than the coordinated free OH peak due to complexation to SO_2, and its parameters are consistent with solvation modes seen in previous studies of ion containing solutions.[43,58,59]

After the removal of SO_2, the interfacial water structure reflects the water composition dictated by SO_2 solubility in the bulk. As displayed in Figure 10, the contribution from the

solution intensity appears to decrease slightly due to interference with the diminishing companion OH peak, but the opposite trend is observed for acid-free solutions where the intensity increases with increased adsorption of SO_2 (Figure 5). The intensity increase for acid-free water is attributed to the reactive
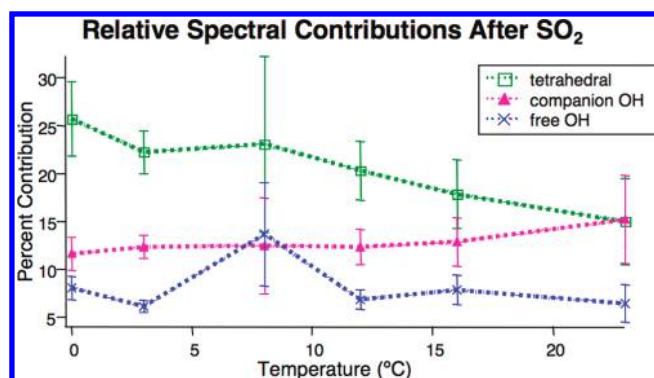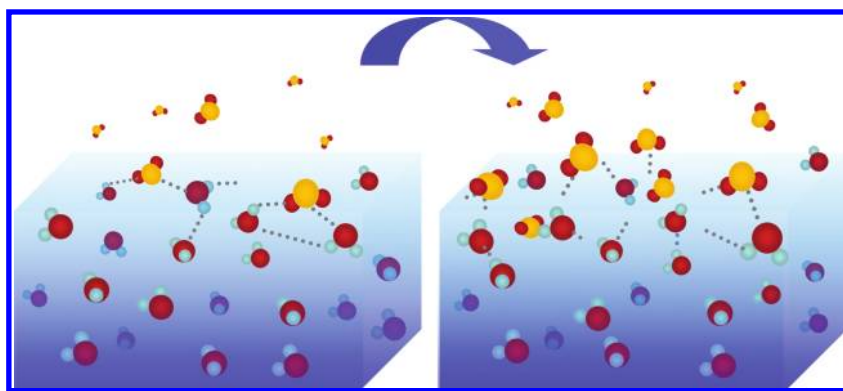
Figure 11. Cartoon representation of the SO_2 (yellow and red):H_2O (light blue and red) interface. When the temperature is cooled (right) from room temperature (left), more SO_2 accumulates.

tetrahedral region increases at lower temperature, consistent with the expected increase in HSO_3^- concentration. That the free and companion OH peaks stay relatively constant with temperature indicates that temperature has no effect on the structure of the topmost water layer in the absence of SO_2. The surface SO_2 complex is reversible throughout the temperature region studied here and does not persist after the gas is removed from the system.

CONCLUSIONS

The uptake of gases by aqueous aerosols is a primary step in many atmospheric interactions, but details about the mechanisms that drive gas adsorption to water remain a mystery. While surface complexes are known to form between SO_2 and H_2O, previous studies have left many questions regarding the behavior of these interfacial species unanswered. Many of the ambiguities found in earlier studies resulted from indirect indicators of surface complexation. The studies presented here provide the first direct examination of surface SO_2:H_2O complexation as a function of temperature and as a function of solution acidity, conditions relevant to tropospheric surface reactions.

The SO_2:H_2O surface complexation observed at room temperature in previous studies[42,43] is significantly enhanced when the temperature is lowered. Whereas at room temperature only a fraction of topmost surface water molecules complex with SO_2, as the temperature is lowered to 0 °C nearly all of the surface water molecules with their free OH bonds protruding into the air complex with SO_2. Although it is known that bulk absorption of SO_2 increases with decreased temperature, this is the first evidence that the intermediate step to this uptake, surface complexation, is also enhanced. Complexation with water molecules in the topmost layer is accompanied by changes in the orientation of the SO_2 bound water molecules prior to the eventual dissolution and reactivity in the bulk aqueous phase. However, even at the lower temperatures, surface complex formation does not necessarily lead to accommodation into the bulk solution as evidenced by the reversible nature of the surface complex formation when the ambient gas is removed. Figure 11 provides a simple depiction of SO_2:water surface complexation. Computational studies are in progress to provide further details into the structure of these surface complexes as a function of temperature.

Important new insights into the adsorption and uptake of SO_2 to acid solutions are also provided in these studies. It is well-known that the uptake of SO_2 is diminished as an aqueous solution becomes more acidic. These studies show that even though the acidic ions in a bulk H_2SO_4 solution are present in the interfacial region, as manifested through their impact on the hydrogen-bonding characteristics water molecules therein, the presence of these ions has no effect on the complexation of SO_2 to the water surface at either room temperature or 0 °C. Furthermore, the increased production of ions such as HSO_3^- in the interfacial region that is observed upon exposure of SO_2 to neutral solutions is not observed in the presence of acid. Hence, the chemistry occurring in the interfacial region is clearly driven by the same equilibrium behavior as the bulk solution. This overall suggests that the complexation behavior at the topmost layer of the surface is largely uncoupled from the rest of the interfacial region and the bulk solution. Because these are the first studies that have been able to probe such detail about surface complexation and its relationship to bulk reactivity, it remains to be seen whether this behavior is unique to surface water complex formation.

From these results, we conclude that low atmospheric temperatures and the acidic conditions common in aqueous aerosols favor surface accumulation of SO_2. The aqueous surfaces can act as as reservoir for SO_2 (or other gases) in the atmosphere by forming interfacial complexes even when the aqueous composition might otherwise impede uptake. This study shows clear evidence of surface accumulation in the absence of bulk absorption, a phenomenon that has important implications for atmospheric chemistry. Surfaces form a platform for potential reactions with either gas-phase or solvated species. These potential surface interactions may be especially relevant to polluted environments where there is an abundance of both SO_2 and reactive organic species. Under such conditions, aqueous surface affinity may lead to surface complexation, increasing the probability of reactions between otherwise noninteractive gases.

AUTHOR INFORMATION

Corresponding Author
richmond@uoregon.edu

ACKNOWLEDGMENT

■ REFERENCES

(1) Finlayson-Pitts, B. J.; Pitts, J. N., Jr. *Chemistry of the Upper and Lower Atmosphere*; Academic Press: San Diego, CA, 2000.

(2) Finlayson-Pitts, B. J. *Chem. Rev.* **2003**, *103*, 4801–4822.

(3) Manahan, S. E. *Environmental Chemistry*, 6th ed.; Lewis Publishers: Boca Raton, FL, 1994.

(4) Allara, D. L. *Nature* **2005**, *437*, 638–639.

(5) Mundy, C. J.; Kuo, I.-F. W. *Chem. Rev.* **2006**, *106*, 1282–1304.

(6) Nathanson, G. M.; Davidovits, P.; Worsnop, D. R.; Kolb, C. E. *J. Phys. Chem.* **1996**, *100*, 13007–13020.

(7) Nathanson, G. M. *Annu. Rev. Phys. Chem.* **2004**, *55*, 231–255.

(8) Garrett, B. C.; Schenter, G. K.; Morita, A. *Chem. Rev.* **2006**, *106*, 1355–1374.

(9) Davidovits, P.; Kolb, C. E.; Wiliams, L. R.; Jayne, J. T.; Worsnop, D. R. *Chem. Rev.* **2006**, *106*, 1323–1354.

(10) Molina, M. J.; Molina, L. T.; Kolb, C. E. *Annu. Rev. Phys. Chem.* **1996**, *47*, 327–367.

(11) Vácha, R.; Slavíček, P.; Mucha, M.; Finlayson-Pitts, B. J.; Jungwirth, P. *J. Phys. Chem. A* **2004**, *108*, 11573–11579.

(12) Worsnop, D. R.; Zahniser, M. S.; Kolb, C. E.; Gardner, J. A.; Watson, L. R.; Van Doren, J. M.; Jayne, J. T.; Davidovits, P. *J. Phys. Chem.* **1989**, *93*, 1159–1172.

(13) Chu, L.; Diao, G.; Chu, L. T. *J. Phys. Chem. A* **2000**, *104*, 7565–7573.

(14) Conklin, M. H.; Bales, R. C. *J. Geophys. Res.* **1993**, *98*, 16851–16855.

(15) Koliadima, A.; Kapolos, J.; Farmakis, L. *Instrum. Sci. Technol.* **2009**, *37*, 274–283.

(16) Boniface, J.; Shi, Q.; Li, T. Q.; Cheung, J. L.; Rattigan, O. V.; Davidovits, P.; Worsnop, D. R.; Jayne, J. T.; Kolb, C. E. *J. Phys. Chem. A* **2000**, *104*, 7502–7510.

(17) Jia, L.; Peng, X. *Heat Transfer—Asian Res.* **2004**, *33*, 219–228.

(18) Jayne, J. T.; Davidovits, P.; Worsnop, D. R.; Zahniser, M. S.; Kolb, C. E. *J. Phys. Chem.* **1990**, *94*, 6041–6048.

(19) Schwartz, S. E.; Freiburg, J. E. *Atmos. Environ.* **2007**, *41*, S138–S153.

(20) Huang, C.-H. *J. Environ. Sci. Health* **2005**, *40*, 2027–2039.

(21) Hsu, C.-T.; Shih, S.-M. *Can. J. Chem. Eng.* **1994**, *72*, 256–261.

(22) Andreasen, A.; Mayer, S. *Energy Fuels* **2007**, *21*, 3274–3279.

(23) Krissman, J.; Siddiqi, M. A.; Lucas, K. *Fluid Phase Equilib.* **1997**, *141*, 221–233.

(24) Worsnop, D. R.; Jayne, J. T.; Kolb, C. E.; Shi, Q.; Boniface, J.; Li, Y. Q.; Rattigan, O. V.; Swartz, E.; Davidovits, P. *J. Aerosol Sci.* **1998**, *29*, s987–s988.

(25) Rattigan, O. V.; Boniface, J.; Swartz, E.; Davidovits, P.; Jayne, J. T.; Kolb, C. E.; Worsnop, D. R. *J. Geophys. Res.* **2000**, *105*, 2065–29078.

(26) Rodriguez-Sevilla, J.; Alvarez, M.; Liminana, G.; Diaz, M. C. *J. Chem. Eng. Data* **2002**, *47*, 1339–1345.

(27) Millero, F. J.; Hershey, P.; Johnson, G.; Zhang, J.-Z. *J. Atmos. Chem.* **1989**, *8*, 377–389.

(28) Zimmermann, K.; Pasel, C.; Lukas, M.; Herbell, J.-D. *Fluid Phase Equilib.* **2009**, *279*, 105–114.

(29) Knipping, E. M.; Lakin, M. J.; Jungwirth, P.; Tobias, D. J.; Gerber, R. B.; Dabdub, D.; Finlayson-Pitts, B. J. *Science* **2000**, *288*, 301–306.

(30) Hu, J. H.; Shi, Q.; Davidovits, P.; Worsnop, D. R.; Zahniser, M. S.; Kolb, C. E. *J. Phys. Chem.* **1995**, *99*, 8768–8776.

(31) George, C.; Behnke, W.; Scheer, V.; Zetzsch, C.; Magi, L.; Ponche, J. L.; Mirabel, P. *Geophys. Res. Lett.* **1995**, *22*, 1505–1508.

(32) Krissman, J.; Siddiqi, M. A.; Lucas, K. *Chem. Eng. Technol.* **1998**, *21*, 641–644.

(33) Laskin, A.; Gaspar, D. J.; Wang, W.; Hunt, S. W.; Cowin, J. P.; Colson, S. D.; Finlayson-Pitts, B. J. *Science* **2003**, *301*, 340–344.

(34) Alexandrova, S.; Marion, M.; Lepinasse, E.; Saboni, A. *Chem. Eng. Technol.* **2004**, *27*, 676–680.

(35) Adema, E. H.; Heeres, P. *Atmos. Environ.* **1995**, *29*, 1091–1103.

(36) Vázquez, G.; Antorrena, G.; Chenlo, F.; Alvarez, E. *Chem. Biochem. Eng. Q.* **1991**, *5*, 163–167.

(37) Chang, C. S.; Rochelle, G. T. *AIChE J.* **1981**, *27*, 292–298.

(38) Matteson, M. J.; Giardina, P. J. *Environ. Sci. Technol.* **1974**, *8*, 50–55.

(39) Shaka, H.; Robertson, W. H.; Finlayson-Pitts, B. J. *Phys. Chem. Chem. Phys.* **2007**, *9*, 1980–1990.

(40) Allen, H. C.; Raymond, E. A.; Richmond, G. L. *J. Phys. Chem. A* **2001**, *105*, 11649–1655.

(41) Cotton, F. A.; Wilkinson, G.; Murillo, C. A.; Bochmann, M. *Advanced Inorganic Chemistry*, 6th ed.; John Wiley and Sons, Inc.: New York, 1999.

(42) Tarbuck, T. L.; Richmond, G. L. *J. Am. Chem. Soc.* **2005**, *127*, 16806–16807.

(43) Tarbuck, T. L.; Richmond, G. L. *J. Am. Chem. Soc.* **2006**, *128*, 3256–3267.

(44) Baer, M.; Mundy, C. J.; Chang, T.-M.; Tao, F.-M.; Dang, L. X. *J. Phys. Chem. B* **2010**, *114*, 7245–7249.

(45) Schriver-Mazzuoli, L.; Chaabouni, H.; Schriver, A. *J. Mol. Struct.* **2003**, *644*, 151–164.

(46) Hirabayashi, S.; Ito, F.; Yamada, K. M. T. *J. Chem. Phys.* **2006**, *125*, 034508/1–034508/6.

(47) Gardner, J. A.; Watson, L. R.; Adewuyi, Y. G.; Van Doren, J. M.; Davidovits, P.; Worsnop, D. R.; Zahniser, M. S.; Kolb, C. E. In *Biogenic Sulfur in the Environment*; Saltzman, E. S., Cooper, W. J., Eds.; ACS Symposium Series; American Chemical Society: Washington, DC, 1989; Vol. 393, Chapter 32, pp 504−517.

(48) Zhang, Z.; Ewing, G. E. *Spectrochim. Acta, Part A* **2002**, *58*, 2105–2113.

(49) Matsumura, K.; Lovas, F. J.; Suenram, R. D. *J. Chem. Phys.* **1989**, *91*, 5887–5894.

(50) Donaldson, D. J.; Guest, J. A.; Goh, M. C. *J. Phys. Chem.* **1995**, *99*, 9313–9315.

(51) Yang, H.; Wright, N. J.; Gagnon, A. M.; Gerber, R. B.; Finlayson-Pitts, B. J. *Phys. Chem. Chem. Phys.* **2002**, *4*, 1832–1838.

(52) Voegele, A. F.; Tautermann, C. S.; Rauch, C.; Loerting, T.; Liedl, K. R. *J. Phys. Chem. A* **2004**, *108*, 3859–3864.

(53) Steudel, R.; Steudel, Y. *Eur. J. Inorg. Chem.* **2009**, 1393–1405.

(54) Cukras, J.; Sadlej, J. *J. Mol. Struct. (THEOCHEM)* **2007**, *819*, 41–51.

(55) Cukras, J.; Sadlej, J. *Pol. J. Chem.* **2008**, *82*, 675–685.

(56) Madsen, M. S.; Gross, A.; Falsig, H.; Kongsted, J.; Osted, A.; Mikkelson, K. V.; Christiansen, O. *Chem. Phys.* **2008**, *348*, 21–30.

(57) Raymond, E. A.; Tarbuck, T. L.; Brown, M. G.; Richmond, G. L. *J. Phys. Chem. B* **2003**, *107*, 546–556.

(58) Raymond, E. A.; Richmond, G. L. *J. Phys. Chem. B* **2004**, *108*, 5051–5059.

(59) Tarbuck, T. L.; Ota, S. T.; Richmond, G. L. *J. Am. Chem. Soc.* **2006**, *128*, 14519–14527.

(60) Richmond, G. L. *Chem. Rev.* **2002**, *102*, 2693–2724.

(61) Bloembergen, N. *Nonlinear Optics*; W. A. Benjamin, Inc.: New York, 1965.

(62) Vidal, F.; Tadjeddine, A. *Rep. Prog. Phys.* **2005**, *68*, 1095–1127.

(63) Buck, M.; Himmelhaus, M. *J. Vac. Sci. Technol., A* **2001**, *19*, 2717–2736.

(64) Hemminger, J. C. *Int. Rev. Phys. Chem.* **1999**, *18*, 387–417.

(65) Lambert, A. G.; Davies, P. B.; Neivandt, D. J. *Appl. Spectrosc. Rev.* **2005**, *40*, 103–145.

(66) Guyot-Sionnest *Surf. Sci.* **2005**, *585*, 1–2.

(67) Voges, A. B.; Al-Abadleh, H. A.; Geiger, F. M. In *Environmental Catalysis*; Grassian, V. H., Ed.; Taylor and Francis: Boca Raton, FL, 2005.

(68) Rao, Y.; Song, D.; Turro, N. J.; Eisenthal, K. B. *J. Phys. Chem. B* **2008**, *112*, 13572–13576.

(69) Bloembergen, N. *Opt. Acta* **1966**, *13*, 311–322.

(70) Ji, N.; Ostroverkhov, V.; Shiu, Y.-J.; Shen, Y.-R. *J. Am. Chem. Soc.* **2006**, *128*, 8845–8848.

(71) Shen, Y. R.; Ostroverkhov, V. *Chem. Rev.* **2006**, *106*, 1140–1154.

(72) Ishibashi, T.-A.; Onishi, H. *Appl. Spectrosc.* **2002**, *56*, 1298–1302.

(73) Ostroverkhov, V.; Waychunas, G. A.; Shen, Y. R. *Phys. Rev. Lett.* **2005**, *94*, 046102/1–046102/4.

(74) Shen, Y. R. *Pure Appl. Chem.* **2001**, *73*, 1589–1598.

(75) Miranda, P. B.; Shen, Y. R. *J. Phys. Chem. B* **1999**, *103*, 3292–3307.

(76) Hirose, C.; Akamatsu, N.; Domen, K. *Appl. Spectrosc.* **1992**, *46*, 1051–1072.

(77) Fourkas, J. T.; Walker, R. A.; Can, S. Z.; Gershgoren, E. *J. Phys. Chem. C* **2007**, *111*, 8902–8915.

(78) Zhu, X. D.; Suhr, H.; Shen, Y. R. *Phys. Rev. B* **1987**, *35*, 3047–3049.

(79) Bloembergen, N.; Pershan, P. S. *Phys. Rev.* **1962**, *128*, 606–622.

(80) Shen, Y. R. *Nature* **1989**, *337*, 519–525.

(81) Bain, C. D. *J. Chem. Soc., Faraday Trans.* **1995**, *91*, 1281–1296.

(82) Löbau, J.; Wolfrum, K. *J. Opt. Soc. Am. B* **1997**, *14*, 2505–2512.

(83) McGall, S. J.; Davies, P. B.; Neivandt, D. J. *J. Phys. Chem. B* **2004**, *108*, 16030–16039.

(84) Shultz, M. J. In *Advances in Multi-Photon Processes and Spectroscopy*; Lin, S. H., Villaeys, A. A., Fujimura, Y., Eds.; World Scientific Publishing Co.: River Edge, NJ, 2008; Vol. 18, Chapter 4, pp 133−199.

(85) Bain, C. D.; Davies, P. B.; Ong, T. H.; Ward, R. N.; Brown, M. A. *Langmuir* **1991**, *7*, 1563–1566.

(86) Gragson, D.; McCarty, B.; Richmond, G. L.; Alavi, D. S. *J. Opt. Soc. Am. B* **1996**, *13*, 1075–2083.

(87) Gragson, D.; Alavi, D.; Richmond, G. L. *Opt. Lett.* **1995**, *20*, 1991–1993.

(88) Raymond, E. A.; Tarbuck, T. L.; Richmond, G. L. *J. Phys. Chem. B* **2002**, *106*, 2817–2820.

(89) Du, Q.; Superfine, R.; Freysz, E.; Shen, Y. *Phys. Rev. Lett.* **1993**, *70*, 2313–2316.

(90) Perry, A.; Neipert, C.; Ridley, C.; Space, B.; Moore, P. B. *Phys. Rev. E: Stat., Nonlinear, Soft Matter Phys.* **2005**, *71*, 050601/1–050601/4.

(91) Smits, M.; Ghosh, A.; Sterrer, M.; Müller, M.; Bonn, M. *Phys. Rev. Lett.* **2007**, *98*, 098302/1–09802/4.

(92) Sovago, M.; Campen, R. K.; Bakker, H. J.; Bonn, M. *Chem. Phys. Lett.* **2009**, *470*, 7–12.

(93) Sovago, M.; Campen, R. K.; Wurpel, G. W. H.; Müller, M.; Bakker, H. J.; Bonn, M. *Phys. Rev. Lett.* **2008**, *100*, 173901/1–173901/4.

(94) Buch, V. *J. Phys. Chem. B* **2005**, *109*, 17771–17774.

(95) Dang, L. X.; Chang, T.-M. *J. Chem. Phys.* **1997**, *106*, 8149–8159.

(96) Auer, B. M.; Skinner, J. L. *J. Chem. Phys.* **2008**, *129*, 214705/1–214705/14.

(97) Tian, C.-S.; Shen, Y. R. *J. Am. Chem. Soc.* **2009**, *131*, 2790–2791.

(98) Tian, C. S.; Shen, Y. R. *Chem. Phys. Lett.* **2009**, *470*, 1–6.

(99) Fan, Y.; Chen, X.; Yang, L.; Cremer, P. S.; Gao, Y. Q. *J. Phys. Chem. B* **2009**, *113*, 11672–11679.

(100) Morita, A. *J. Phys. Chem. B* **2006**, *110*, 3158–3163.

(101) Kuo, I.-F. W.; Mundy, C. J.; Eggimann, B. L.; McGrath, M. J.; Siepmann, J. I.; Chen, B.; Vieceli, J.; Tobias, D. J. *J. Phys. Chem. B* **2006**, *110*, 3738–3746.

(102) Walker, D. S.; Hore, D. K.; Richmond, G. L. *J. Phys. Chem. B* **2006**, *110*, 20451–20459.

(103) Ishiyama, T.; Morita, A. *J. Phys. Chem. C* **2007**, *111*, 721–737.

(104) Walker, D. S.; Richmond, G. L. *J. Phys. Chem. C* **2007**, *111*, 8321–8330.

(105) Ishiyama, T.; Morita, A. *J. Phys. Chem. C* **2007**, *111*, 738–748.

(106) Hore, D. K.; Walker, D. S.; Richmond, G. L. *J. Am. Chem. Soc.* **2008**, *130*, 1800–1801.

(107) Ishiyama, T.; Morita, A. *J. Phys. Chem. C* **2009**, *113*, 16299–16302.

(108) Ishiyama, T.; Morita, A. *J. Chem. Phys.* **2009**, *131*, 244714/1–244717/17.

(109) Noah-Vanhoucke, J.; Smith, J. D.; Geissler, P. L. *J. Phys. Chem. B* **2009**, *113*, 4065–4074.

(110) Auer, B. M.; Skinner, J. L. *Chem. Phys. Lett.* **2009**, *470*, 13–20.

(111) Kühn, T. D.; Pascal, T. A.; Kaxiras, E.; Jung, Y. *J. Phys. Chem. Lett.* **2011**, *2*, 105–113.

(112) Gan, W.; Wu, D.; Zhang, Z.; Feng, R.-r.; Wang, H.-f. *J. Chem. Phys.* **2006**, *124*, 114705/1–114705/15.

(113) Morita, A.; Hynes, J. T. *J. Phys. Chem. B* **2002**, *106*, 673–685.

(114) Ghosh, A.; Smits, M.; Sovago, M.; Bredenbeck, J.; Müller, M.; Bonn, M. *Chem. Phys.* **2008**, *350*, 23–30.

(115) Auer, B. M.; Skinner, J. L. *J. Phys. Chem. B* **2009**, *113*, 4125–4130.

(116) Bakker, H. J.; Skinner, J. L. *Chem. Rev.* **2010**, *110*, 1498–1517.

(117) Sovago, M.; Vartiainen, E. M.; Bonn, M. *J. Phys. Chem. C* **2009**, *113*, 6100–6106.

(118) Tian, C. S.; Shen, Y. R. *Phys. Rev. Lett.* **2008**, *101*, 139401/1.

(119) Sovago, M.; Campen, R. K.; Wurpel, G. W. H.; M uller, M.; Bakker, H. J.; Bonn, M. *Phys. Rev. Lett.* **2008**, *101*, 139402/1.

(120) Stiopkin, I. V.; Jayathilake, H. D.; Bordenyuk, A. N.; Benderskii, A. V. *J. Am. Chem. Soc.* **2008**, *130*, 2271–2275.

(121) Schnitzer, C.; Baldelli, S.; Shultz, M. J. *J. Phys. Chem. B* **2000**, *104*, 585–590.

(122) Wei, X.; Miranda, P. B.; Shen, Y. R. *Phys. Rev. Lett.* **2001**, *86*, 1554–1557.

(123) Wei, X.; Shen, Y. R. *Appl. Phys. B: Lasers Opt.* **2002**, *74*, 617–620.

(124) Shen, Y. R. *Solid State Commun.* **1998**, *108*, 399–406.

(125) Baldelli, S.; Schnitzer, C.; Shultz, M. J. *Chem. Phys. Lett.* **1999**, *302*, 157–163.

(126) Levering, L. M.; Sierra-Hernández; Allen, H. C. *J. Phys. Chem. C* **2007**, *111*, 8814–8826.

(127) Tian, C.; Ji, N.; Waychunas, G. A.; Shen, Y. R. *J. Am. Chem. Soc.* **2008**, *130*, 13033–13039.

(128) Miyamae, T.; Morita, A.; Ouchi, Y. *Phys. Chem. Chem. Phys.* **2008**, *10*, 2010–2013.

(129) Baldelli, S.; Schnitzer, C.; Campbell, D. J.; Shultz, M. J. *J. Phys. Chem. B* **1999**, *103*, 2789–2795.

(130) Schnitzer, C.; Baldelli, S.; Shultz, M. J. *Chem. Phys. Lett.* **1999**, *313*, 416–420.

(131) Baldelli, S.; Schnitzer, C.; Shultz, M. J.; Campbell, D. J. *Chem. Phys. Lett.* **1998**, *287*, 143–147.

(132) Baldelli, S.; Schnitzer, C.; Shultz, M. J. *J. Phys. Chem. B* **1997**, *101*, 10435–10441.

(133) Radüge, C.; Pflumio, V.; Shen, Y. R. *Chem. Phys. Lett.* **1997**, *274*, 149–144.

(134) Shultz, M. J.; Baldelli, S.; Schnitzer, C.; Simonelli, D. *J. Phys. Chem. B* **2002**, *106*, 5313–5324.